A new Heusler compound Cu_2FeAl:
electronic structure, magnetism and transport properties

Ming Zhang[*, 1], **Yuting Cui**[1], **Zhuhong Liu**[1], **Guodong Liu**[1], **Jinglan Chen**[1],
Guangheng Wu[1], **Yu Sui**[2], **Yuqiang Liu**[2], **Zhengnan Qian**[2], **E. Brück**[3], and **F. R. de Boer**[3]

[1] State Key Laboratory for Magnetism, Institute of Physics, Chinese Academy of Sciences,
  Beijing 100080, People's Republic of China
[2] Center for the Condensed-Matter Science and Technology, Department of Physics,
  Harbin Institute of Technology, Harbin 150001, People's Republic of China
[3] Van der Waals-Zeeman Instituut, Universiteit van Amsterdam, Valckenierstraat 67,
  1018XE Amsterdam, The Netherlands

The new ferromagnetic Heusler alloy of Cu_2FeAl has been prepared by melt spinning. The band-structure calculations on this alloy predict a ferromagnetic ground state and the crystal structure not to be stable. The intrinsic properties of Cu_2FeAl ribbons are described from magnetic and transport measurements. The electronic structure calculations show that the magnetic moment of Cu_2FeAl is not localized, which is not the same as Cu_2MnAl. At low temperature, the magnetization decreases as $T^{3/2}$, as can be well interpreted by spin-wave theory. An interpretation is given for the electrical resistivity and leads to information about the microscopic scattering mechanisms involved. A negative longitudinal magnetoresistance of less than 1% at high field is observed, which can be qualitatively explained by s-d interaction. The magnetic resistivity is estimated for this compound.

1 Introduction

Heusler alloys [1–3] are ternary intermetallic compounds with stoichiometric composition X_2YZ, where X and Y can be transition elements, and Z is an sp element. Heusler alloys become more and more attractive nowadays, because they have shown many useful properties for applications, such as the ferromagnetic shape memory effect [4] and ferromagnetic half-metal behaviour [5–7]. They are also interesting for magnetism research: the magnetic properties strongly depend on both conduction electron concentration [8] and chemical order [9]. Up to now, however, the ferromagnetism of X_2FeZ-type Heusler alloys has rarely been investigated. The formation and the coupling of the magnetic moments in Fe-related Heusler alloys are still an attractive subject for theoretical and experimental investigations. But the problem is that, so far, Fe-related Heusler alloys with non-magnetic X and Z elements have rarely been found. This is because the Fe compounds are not easy to synthesize even if the Mn-related alloy is known to exist.

In this work, we successfully prepared a unique Heusler alloy of Cu_2FeAl by utilizing the melt-spinning method. This alloy provides a good system to investigate the formation and the coupling between iron magnetic moments, as Cu and Al are both non-ferromagnetic elements. Furthermore, it is worth to mention that the meta-stable ferromagnetic state of this compound seems to be related to the $L2_1$ phase instability.

[*] Corresponding author: e-mail: zm_info@yahoo.com.cn, Phone: +86 10 8264 9247, Fax: +86 10 8264 9485

2 Computational and experimental details

The linearized-augmented plane wave plus local orbitals method based on the local spin density approximation (LSDA) for the exchange-correlation potential within the framework of DFT [10] is used in our calculations. The relativistic effect is taken into account in the scalar approximation, but the spin-orbital coupling is neglected. The muffin-tin sphere radii R used are 2.4 a.u. for Cu, Fe and Al atoms. Inside the atomic spheres the charge density and the potential are expanded in crystal harmonics up to $l = 6$. The radial basis functions of each LAPW are calculated up to $l = 8$ and the non-spherical potential contribution to the Hamilton matrix has an upper limit of $l = 4$. The Brillouin-zone integration is done with a modified tetrahedron method [11] and we use 60 k-points in the first irreducible Brillouin zone (IBZ). The density plane-wave cutoff is $RK_{max} = 8.0$. The self-consistency is better than 0.001 me/a.u.^{3} for charge density and spin density, and the stability is better than 0.01 mRy for the total energy per unit cell.

The ingots are prepared by repeated melting of high-purity Cu, Fe and Al metals in an arc furnace with argon atmosphere protection and subsequently are broken up. Some are annealed in vacuum at 800 °C for five days and others are used for melt-spinning. The melt-spun ribbons are prepared by a single wheel technique with the substrate velocity (V_s) of 20 m/s, under a protective Ar atmosphere. X-ray diffraction (XRD) spectra are performed to identify the crystallographic structure. Magnetization is measured using a SQUID magnetometer. The electrical resistivity and the magnetoresistance measurements are carried out using the four-point DC technique.

3 Result and discussion

3.1 Density of states

3.1.1 Total energy and lattice constant

To determine the theoretical lattice parameter, the band calculations are performed and the total energy for Cu_2FeAl with the ferromagnetic configuration as a function of the lattice parameter is shown in Fig. 1. The theoretical value of the lattice parameter, $a = 0.5934$ nm, is determined by minimizing the total energy. Here we have to note that the equilibrium lattice parameter predicted by LDA calculation is underestimated by a few percent (less than 3%) due to the so-called overbinding effect [12].

3.1.2 Density of states

We calculate the spin-dependent total and the partial DOS of Cu_2FeAl. Figure 2a shows the total DOS. For minority-spin electrons, the main features are the two high-density regions widely separated by a low-density region, but the Fermi level is situated within a high-density region. The partial density of states is shown in Fig. 2b. It is clear that the Fe and Cu 3d states behave quite differently. The region
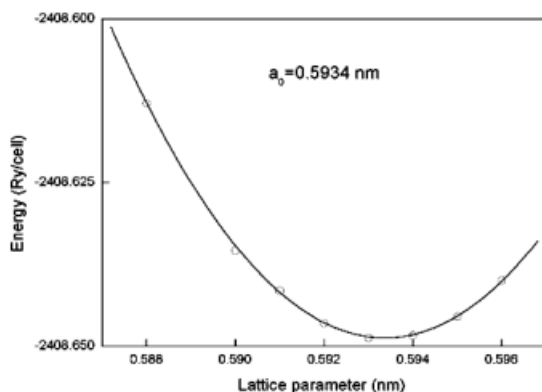
**Fig. 1** Calculated lattice parameter dependence of the total energy.
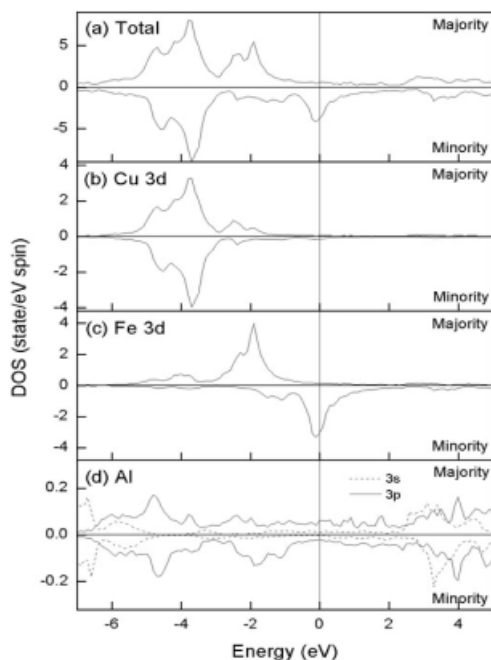
Fig. 2 Calculated spin-projected total DOS (a) and partial DOS of Cu *3d* (b), Fe *3d* (c), and Al *3s* (dashed line), *3p* (solid line). The Fermi level is marked by a vertical solid line. Note that the remarks of majority and minority designate the majority-spin electrons and the minority-spin electrons, respectively.

between –5 eV to –3 eV consists mainly of Cu *3d* states, and is almost identical for majority and minority spin directions, so Cu *3d* states are almost occupied. The Fe *3d* majority-spin states are located at a higher binding energy and we observe a clear splitting between minority and majority states. As described in the paper dealing with the band structure of Ni_3Mn [13] and Cu_2MnAl [14], it is highly probable that the separation of bonding and antibonding orbitals by a low-density region, in which the Fermi level is situated, stabilizes the ferromagnetic state. But in our calculation, the Fermi level is situated in the antibonding region and this situation will in general lead to an unstable ferromagnetic state. Tobola et al. [15] indicated that, as a consequence of such DOS behaviour, the total energy of the system would be strongly augmented, and a different crystal structure would be favourable in energy. This may be the reason why, as shown in the following X-ray diffraction pattern, the pure $L2_1$ phase of Cu_2FeAl cannot be obtained by using the ordinary melting and annealing process. On the other hand, our melt-spinning technique seems to be an effective way to prepare this phase. In fact, some new materials with similar characters, such as NiFeSb and Ni_2FeGa have recently been successfully manufactured in our laboratory [16, 17].

The characteristic of DOS in Fig. 2a can be interpreted qualitatively by comparing DOS of Cu_2FeAl with that of Cu_2MnAl [14]. In the DOS of Cu_2MnAl [14], the high density regions for majority and minority spin Cu *d* states are situated in the lower energy range with respect to those of Mn, therefore Cu *d*-bands are almost occupied, as is similar to that of Cu_2FeAl. In contrast, in the partial DOS of Mn, the majority-spin bands are nearly fully occupied whereas the minority-spin bands are not occupied. The Fermi level is situated in a low-density region. In the case of Cu_2FeAl, there is one valence electron more than that of Cu_2MnAl, the two spin states of Cu and the majority-spin states of Fe are already fully occupied as in Cu_2MnAl; thus the additional electron has to be screened by the minority Fe *d* states, so that the Fermi level falls into the minority Fe states.

As shown in Fig. 2, the Fe majority-spin *d* states are almost completely occupied and the bandwidth indicates that they are delocalized. The total magnetic moment in Bohr magneton is just the difference between the majority-spin and minority-spin occupied states. Unlike the X_2MnZ-type Heusler alloys, the minority-spin *d* electrons of Fe cannot be excluded from the Fe site and the Fe minority-spin *d* states, however, are partly occupied. Hence, this DOS behaviour indicates that the magnetic moment of Cu_2FeAl is not localised, it is different from that of Cu_2MnAl. The magnetic moments of the Cu, Fe and
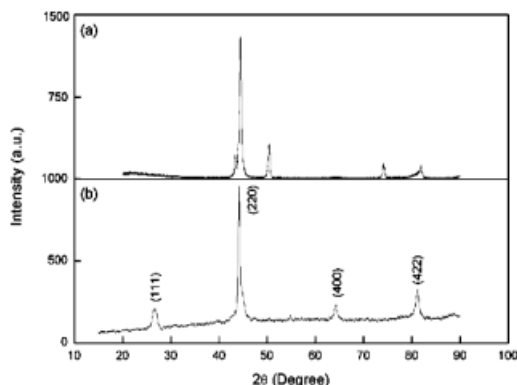
**Fig. 3** X-ray diffraction spectra for the precursor ingot (a) and the spun-ribbon (b) of Cu_2FeAl compound.

Al atoms are $0.027\mu_B$, $2.362\mu_B$ and $-0.038\mu_B$, respectively. Thus the total spin magnetic moment per formula unit is equal to 2.378 μ_B. From the density of states at the Fermi level ($N(E_F) = 4.380$ states/eV · cell) of both spin bands and using independent-electron theory, the coefficient γ of the electronic specific heat ($C = \gamma T$) has been estimated as $\gamma = 10.3$ mJ/mol · K^2.

3.2 X-ray diffraction

Figure 3 shows the XRD patterns of the precursor ingot (a) and melt-spun ribbons in the as-spun state (b). As shown in Fig. 3, no sign of $L2_1$ structure can be found in the melt-ingot samples and the XRD reveals some simple-cubic structure. On the other hand, the $L2_1$ structure in our melt-spun ribbon samples is confirmed. Ordering of the Fe and Al sublattice is indicated by the presence of the (111) superlattice diffraction peak. But the (200) superlattice peak that indicates the ordering of the Cu sublattice is not presented, and the peaks are diffuse. Hence, in Cu_2FeAl lattice there maybe exist some antisite disorder. Indexing all characteristic diffraction peaks, the lattice constant has been determined as 0.5905 nm, which is consistent with our calculated value. This implies that the nearest-neighbour distance between two iron atoms is lager than 0.41 nm. For this large interatomic distance, the direct coupling between iron atoms can be eliminated as an exchange mechanism. Concerning the non-magnetic elements of Cu and Al in the compound, our Cu_2FeAl ribbons with $L2_1$ structure provide a new stage to reveal the indirect exchange interaction in this new Heusler alloy. Our sample preparation also suggests the possibility of fabricating other new Heusler compounds.

3.3 Magnetism

Figure 4 shows the temperature dependence of the magnetization measured using a magnetic balance in a magnetic field of 500 Oe. From the sharp magnetic transitions we derive a Curie temperature (T_c) of
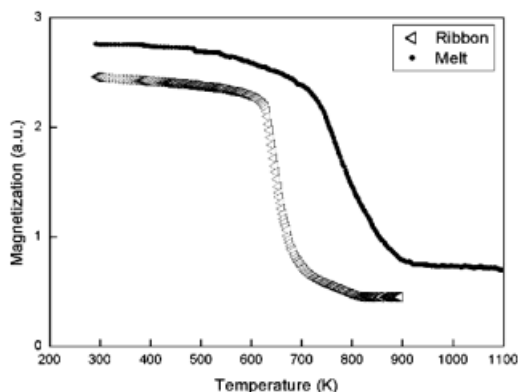
Fig. 4 Temperature dependence of the magnetizations for Cu_2FeAl precursor ingots and ribbons under the field of 500 Oe.
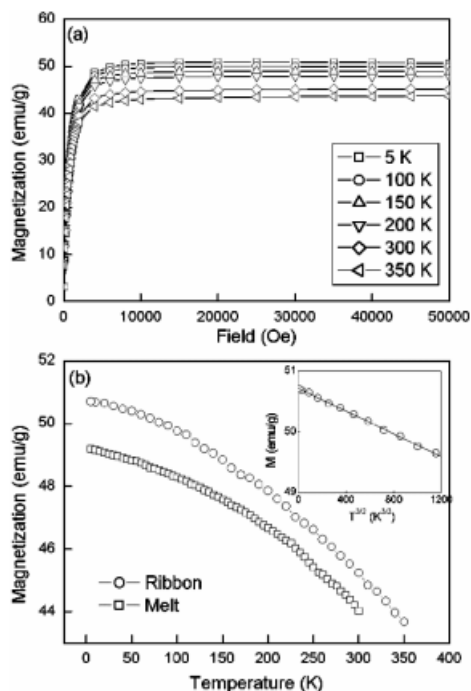
Fig. 5 (a) Magnetization dependence of the magnetic field for Cu$_2$FeAl ribbons at various temperatures. (b) Temperature dependence of magnetizations for precursor ingots and ribbons under the field of 50 kOe. Inset graph shows the ribbon data for $T < 100$ K as a function of $T^{3/2}$. The solid line in the inset graph is a linear fit to the Cu$_2$FeAl data, demonstrating the $T^{3/2}$ dependence of the magnetization for this low T range.

680 K and 870 K for ribbons and precursor ingots, respectively. The magnetization M versus H curves for ribbons is shown in Fig. 5 (a) at $T = 5$, 100, 150, 200, 300 and 350 K, respectively. At 5 K, the magnetization is saturated in the magnetic field of about 1200 Oe, indicating that the compound displays only low magneto-crystalline anisotropy. The saturation moment at 5 K obtained by extrapolation corresponds to $1.94\mu_B$ per formula unit, which is different from the computed result of $2.378\mu_B$. This difference is usually ascribed to atomic disorder and the microstructure defects derived from the melt-spinning process. The magnetic moments of the Heusler alloys are intensively related to the atomic order. Atom anti-site disorder and lattice defects, which usually can be observed in melt-spun ribbons and have been confirmed by the aforementioned XRD measurements and the followed transport experiments (residual resistivity ratio), can influence the electronic structure of Heusler-type alloys remarkably, and accordingly would have a great effect on the magnetic moment. Slebarski et al. [18] reported that the magnetic impurities existed in the lattice due to the atom disorder could lead to the remarkable decrease of the magnetic moment. Furthermore, Sugimoto et al. [19] also reported that the magnetic moment of ribbons could be much smaller than that of the bulks, which could increase as much as two times by the appropriate annealing treatment. Thus, it is expected that the moment of an annealed Cu$_2$FeAl ribbon can be increased and approach the prediction of the LAPW calculation. This work is under way.

The temperature dependence of the saturation magnetization $M(T)$ curves for both the melt spun ribbon and the precursor material are shown in Fig. 5b. At low temperature the curve for Cu$_2$FeAl follows the expression $M(T) = M(0)(1 - AT^n)$ with $n = 1.5$, the value expected from spin-wave theory. The value of A is 1.83×10^{-5} K$^{-3/2}$. Within the spin-wave theory we can calculate the value of the spin-wave stiffness coefficient D in the spin-wave dispersion relation $\hbar\omega = Dq^2$ from the value of A, using the equation $A = 2.612(V/S)(k_B/4\pi D)^{3/2}$ [20], where V is the volume per magnetic atom, S is the spin and k_B is the Boltzmann constant. The value obtained is 166.0 meV Å^2. Figure 5b also shows the temperature dependence of the magnetization for the precursor ingot. In the whole temperature range measured, the saturated magnetization for the precursor ingot is smaller than the magnetization for the ribbons. We guess that this behaviour is probably due to the microstructure defects, but the convincing interpretations of this phenomenon are still unknown.

3.4 Transport properties

Figure 6 shows the temperature dependence of the resistivity. The compound has a residual resistivity ratio (RRR) of $\rho_{300K}/\rho_{5K} = 2.4$, which is much lower than that of single crystal Co$_2$MnSi, 6.5. [9] Small amount of defects and impurities can have dramatic effects on the RRR, and as for the Heusler com-
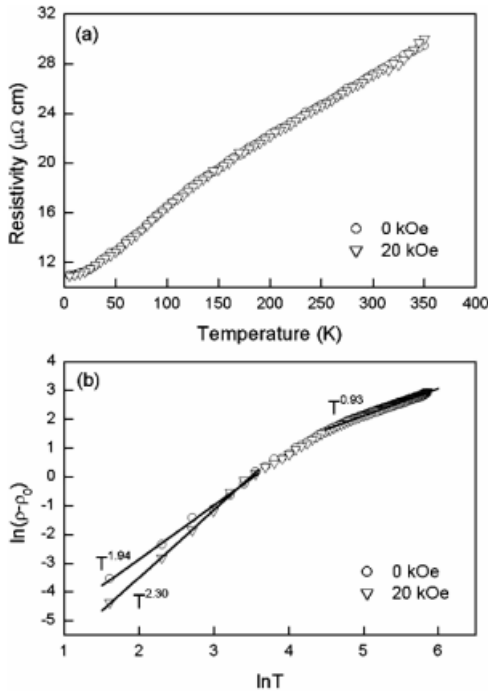
Fig. 6 (a) Temperature dependence of the electrical resistivity for Cu_2FeAl with (triangle) and without (circle) the 2 T field. (b) $\ln(\rho - \rho_0)$ as a function of $\ln(T)$ for the Cu_2FeAl resistivity data with and without the 2 T field. The slope of this curve corresponds to the power law exponent n if we assume the functional form $\rho(T) = \rho_0 + cT^n$. the Cu_2FeAl data, demonstrating the $T^{3/2}$ dependence of the magnetization for this low T range.
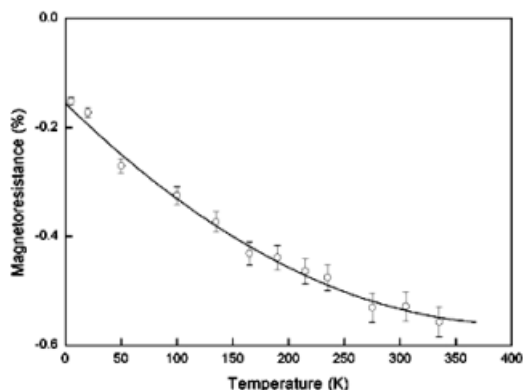
pounds, a reduced RRR can result from scattering contributions from impurities or antisite defects. Raphael et al. [9] reported a Co-Mn antisite disorder of around 10 ~ 14% for the arc-melted sample of Co_2MnSi which RRR has a magnitude of 2.7. Therefore, it is a reasonable estimation that there exist some antisite defects in Cu_2FeAl. According to Matthiessen's rule [21], we separate the total resistivity into its residual and its temperature dependent part as $\rho = \rho_0 + \rho_L(T)$. By assuming the functional form $\rho_L(T) = cT^n$ for our data, a plot of $\ln(\rho - \rho_0)$ as a function of $\ln(T)$ will yield a curve whose slope corresponds to the local power law parameter n. Figure 6 shows that the temperature dependence of the resistivity follows a T^n behavior with $n \approx 1.94$ (close to $n = 2$) below 40 K.

At very low temperatures, possible contributions to the temperature dependence of the resistivity are electron-electron, electron-phonon and electron-magnon scatterings. At low temperatures the electron-phonon scattering can give rise to a well known T^5 dependence and a linear dependence above the Debye temperature [21]. In addition, it is known that, in the case of ferromagnetic elements such as Fe, Co and Ni, the resistivity usually has a term proportional to T^2, which is ascribed to electron-electron scattering of conduction electrons [22, 23]. Watts et al. [24] reported that electron-magnon scattering could also give a T^2 dependence. We can conclude that at very low temperature the effect of the electron-phonon scattering on the resistivity is very small and can be neglected. Furthermore, as seen in Fig. 6, the high-temperature range can be described with the usual linear temperature coefficient.

Figure 6 also shows the temperature dependences of the resistivity in an applied magnetic field $H = 2$ T. The low-temperature power law parameter n increases from 1.94 to 2.30, which is probably due to the lack of the spin fluctuations, spin-disorder or/and magnon excitations in a magnetic field [25]. Figure 7 shows the temperature dependence of the longitudinal magnetoresistance (MR) at a magnetic field of 2 T. The magnitude of MR is small (less than 1%) in the whole temperature range, which may be attributed to the rather high residual resistivity, which is due to the aforementioned defects. As frequently observed in ferromagnets the MR is negative [26]. These are characteristics of MR due to s-d interactions. Briefly, we assert that at the lowest temperatures the energy $g\mu_B H_i$ of an electron in the internal field is larger than $k_B T$ and spin-flip scattering is thus a minimum [27]. Increasing temperature increases $k_B T$ and so opens the spin-flip scattering channels, if $g\mu_B H_i$ and $k_B T$ are of the same order, an applied field will give a large negative MR when the spin-flip channels are open.

The maximum value of the magnetic scattering resistivity, ρ_m^* (defined by Fig. 8 of Ref. [28]), is estimated to be

$$\rho_m^* = \alpha \sum_j p_j \left[\frac{\mu_j}{g}\right]\left[\frac{\mu_j}{g} + 1\right], \tag{1}$$

where p_j is taken as a composition of atom j, and $\alpha = 160$ can give a good fit for the Heusler compounds [28]. Here, the moment μ_j is evaluated from the saturation magnetization. Thus, we can give a rough estimation of the magnetic scattering resistivity of 75 μΩcm, which is obviously reasonable with respect to our experimental data.

4 Summary

The electronic structure calculation shows that the Fermi level situates in the antibonding region, which can lead to an unstable ferromagnetic state, and the magnetic moment of Cu_2FeAl characters delocalized. But it is worth noting from the XRD spectra that the metastable ferromagnetic state and the $L2_1$ structure of Cu_2FeAl can be obtained for the first time by using the melt-spinning technique, which opens a novel approach of searching for new Heusler alloys. The magnetization as a function of temperatures can be explained well by spin-wave theory. The electrical resistivity shows a quadratic temperature dependence at low temperature, which is ascribed to electron-electron scattering of conduction electrons. The effect of the electron-phonon scattering on the resistivity is only significant at elevated temperatures. Furthermore, under a magnetic field sufficient to saturate the magnetic moments, the power law coefficient of the temperature dependence can increase somewhat probably due to the absence of spin fluctuations, spin-disorder scattering and/or magnon excitations in a magnetic field. We record a negative longitudinal magnetoresistance of less than 1%, and a qualitative interpretation is given of the magnetoresistance behaviour according to the *s-d* interaction theory. Finally, the magnetic scattering resistivity has been estimated as 75 μΩcm.

References

[1] F. Heusler, Verh. Dtsch. Phys. Ges. **5**, 219 (1903).
[2] P. J. Webster, Contemp. Phys. **10**, 559 (1969).
[3] C. C. M. Compbell, J. Phys. F **5**, 1931 (1975).
[4] V. V. Khovailo, T. Takagi, J. Tani, R. Z. Levitin, A. A. Cherechukin, M. Matsumoto, and R. Note, Phys. Rev. B **65**, 092410 (2002).
[5] R. A. de Groot, F. M. Mueller, P. G. van Engen, and K. H. J. Buschow, Phys. Rev. Lett. **50**, 2024 (1983).
[6] H. Ebert and G. Schütz, J. Appl. Phys. **69**, 4627 (1991).
[7] P. J. Brown, K. U. Neumann, P. J. Webster, and K. R. A. Ziebeck, J. Phys.: Cond. Matt. **12**, 1827 (2000).
[8] P. J. Webster and M. R. I. Ramadan, J. Magn. Magn. Mater. **13**, 301 (1979).
[9] M. P. Raphael, B. Ravel, Q. Huang, M. A. Willard, S. F. Cheng, B. N. Das, R. M. Stroud, K. M. Bussmann, J. H. Claassen, and V. G. Harris, Phys. Rev. B **66**, 104429 (2002).
[10] U. von Barth and L. Hedin, J. Phys. C **5**, 1629 (1972).
     P. Hohenberg and W. Kohn, Phys. Rev. **136**, B864 (1964).
     P. Blaha, K. Schwarz, P. Sorantin, and S. B. Tricky, Comput. Phys. Commun. **59**, 399 (1990).

[11] P. E. Blöchl, O. Jepson, and O. K. Andersen, Phys. Rev. B **49**, 16223 (1994).
   S. Blugel, H. Akai, R. Zeller, and P. H. Dederichs, Phys. Rev. B **35**, 3271 (1987).
[12] M. Asato, A. Settels, T. Hoshino, T. Asada, S. Blugel, R. Zeller, and P. H. Dederichs, Phys. Rev. B **60**, 5202 (1999).
[13] J. Yamashita, S. Asano, and S. Wakoh, Prog. Theor. Phys. **47**, 774 (1972).
[14] S. Ishida, J. Ishida, S. Asano, and J. Yamashita, J. Phys. Soc. Japan **45**, 1239 (1978).
[15] J. Tobola and J. Pierre, J. Alloys Compd. **296**, 243 (2000).
[16] Z. H. Liu, M. Zhang, Y. T. Cui, Y. Q. Zhou, W. H. Wang, G. H. Wu, X. X. Zhang, and G. Xiao, Appl. Phys. Lett. **82**, 424 (2002).
[17] M. Zhang, Z. H. Liu, H. Hu, Y. T. Cui, G. Liu, J. Chen, G. H. Wu, Y. Sui, Z. Qian, Z. Li, H. Tao, B. Zhao, and H. Wen, Solid State Commun. **128**, 107 (2003).
[18] A. Slebarski, M. B. Maple, E. J. Freeman, C. Sirvent, D. Tworuszka, M. Orzechowska, A. Wrona, A. Jezierski, S. Chiuzbaian, and M. Neumann, Phys. Rev. B **62**, 3296 (2000).
[19] S. Sugimoto, S. Kondo, H. Nakamura, D. Book, Y. Wang, T. Kagotani, R. Kainuma, K. Ishida, M. Okada, and M. Homma, J. Alloys Compd. **265**, 273 (1998).
[20] Y. Noda and Y. Ishikawa, J. Phys. Soc. Japan **40**, 699 (1976).
[21] J. M. Ziman, Electrons and Phonons (Oxford University Press, 1960)
[22] M. J. Otto, R. A. M. van Woerden, P. J. van der Valk, J. Wijngaard, C. F. van Bruggen, and C. Haas, J. Phys.: Condens. Matter **1**, 2351 (1989).
[23] G. K. White and S. B. Woods, Philos. Trans. R. Soc. Lond. A **251**, 273 (1958).
[24] S. M. Watts, S. Wirth, S. von Molnár, A. Barry, and J. M. D. Coey, Phys. Rev. B **61**, 9621 (2000).
[25] G. J. Snyder, R. Hiskes, S. DiCarolis, M. R. Beasley, and T. H. Geballe, Phys. Rev. B **53**, 14434 (1996).
[26] K. Yoshida, Phys. Rev. **107**, 396 (1957).
[27] M. T. Béal-Monod and R. A. Weiner, Phys. Rev. **170**, 552 (1968).
[28] Y. Nishino, S. Inoue, S. Asano, and N. Kawamiya, Phys. Rev. B **48**, 13607 (1993).